International Journal of Adhesion & Adhesives 122 (2023) 103332

Contents lists available at ScienceDirect

International Journal of Adhesion and Adhesives

journal homepage: www.elsevier.com/locate/ijadhadh

Use of DIC in the characterisation of mode II crack propagation in adhesive fatigue testing

Olli Orell *, Jarno Jokinen, Mikko Kanerva

Tampere University, Materials Science and Environmental Engineering, PO Box 589, FI-33101, Tampere, Finland

ARTICLE INFO

Keywords:
Adhesive
Fatigue
Digital image correlation
Mode II
End-notched flexure

ABSTRACT

Adhesively bonded joints are used in many applications which are dynamically loaded. Thus, excellent fatigue properties of adhesives, especially under fracture mode II, are required. The fracture mode II testing of adhesive is challenging, where the observation of the crack length is complicated. Accordingly, compliance-based effective crack length definitions avoiding direct observation have been used instead. The experimental crack monitoring method using digital image correlation (DIC) is studied in this work. The DIC-based monitoring is compared to the compliance-based method in defining the crack length. The developed DIC-based method is useful to study, especially, the microcracked adhesive region ahead of the distinct open crack tip.

1. Introduction

A significant amount of research has been conducted to understand failure in adhesively bonded joints. Static fracture testing has already taken steps towards standardisation. The testing of fracture mode I has already been standardised [1], and the mode II-related standard is being processed. Typically, static mode II testing has been performed using the method of end-notched flexure (ENF) [2], four-point end-notched flexure (4ENF), or the end-loaded split (ELS) [3]. The specimen types have differences in fracture surface friction and stability of crack propagation. Recently, the focus of research has been on the method development for fatigue. The testing for fatigue has mainly been performed using the ENF and ELS specimens.

Fatigue testing of joints is generally more complex than the corresponding quasi-static tests. One of the main challenges in the fatigue testing of adhesives, especially in mode II loaded joints, is the measurement of the crack length. Typically, the experimental methods are based on visual observation of the open crack and using magnifying tools, e.g. microscopes [4]. The visual observation interpretation depends on the observer when the test is performed manually. The manual observation becomes even less attractive when low load levels are used and the testing time is increased. Other techniques not dependent on visual observation are developed, e.g. crack gauges [5]. Clip gauges have been used to determine the crack length in single-lap shear tests [6] and double cantilever beam (DCB) tests [4]. In addition, distributed optical fibre sensors have been used to characterise crack propagation in fatigue testing with step-lap specimens [7].

Generally, the physical crack propagation in mode I testing is defined as the opening of the debonded interface. However, existing plastic deformation adjacent to the crack tip complicates the definition of the precise crack length. The damage related to the plastic-deformed crack tip might result in several micro-crack tips or smear the crack tip beyond the technique used for observation [8]. On the other hand, the crack propagation in mode II testing is even more challenging compared to mode I testing [9]. The mode II crack propagation is seen as a relative sliding of the originally united components in the debonded interface. Several studies have excluded the experimental determination of the crack length in mode II testing. Crack monitoring has been considered overly labour-intensive and inaccurate [10]. The adhesive properties, such as plasticity, strain hardening and relaxation, add complexity [11,12]. The challenges of the crack length have mainly been overcome by developing numerical post-processing methods using beam theory, specimen compliance and equivalent crack-based methodologies [8,10,11,13]. The equivalent crack length analytical approaches have been developed, including the fracture process zone (FPZ), which considers the plasticisation and micro-straining [8] at the crack tip regime.

This paper studies a novel approach to characterise crack propagation using digital image correlation (DIC). The DIC is an optical contactless measuring technique to study surface displacements. The method is already an established tool and is used in various applications, which include material testing [14], component testing [15], particle movement measurements [16] and fracture characteristics [17]. The

* Corresponding author.
E-mail address: olli.orell@tuni.fi (O. Orell).

https://doi.org/10.1016/j.ijadhadh.2023.103332
Received 28 June 2022; Received in revised form 16 December 2022; Accepted 23 January 2023
Available online 4 February 2023

DIC can monitor even tiny details when using an optical setup that can produce high magnification. Here, we have used the DIC-based crack monitoring technique for mode II testing for fatigue by using an ENF-type specimen. However, typically 20–30 mm of crack propagation is observed in ENF fatigue specimens during a single test requiring a relatively large field of view from the used setup. For that reason, the DIC could not be focused locally, only on the crack tip in the adhesive. Instead, the cracked adhesive region was studied by post-processing the determined displacement fields of the adherends similar to the previous work by Jokinen et al. [18]. The crack growth of the epoxy film adhesive FM 300-2, used to join aluminium alloy adherends, was studied under three different load levels. The DIC results were compared to the compliance-based method and the indications by penetrating fluid study. The main target of the work was to study the applicability of the developed crack monitoring method based on the DIC measurements of the adherend deformation.

2. Materials and methods

2.1. Specimen

The ENF specimens in this work consisted of aluminium alloy (Alumec 89, Uddeholm) adherends and the studied adhesive. The adhesive was epoxy film adhesive FM 300-2 by Solvay, which includes a thermoplastic polyester knit carrier. The original aluminium plates were bonded using two adhesive film layers, and the pre-existing crack between the layers was made using PTFE film (thickness 20 μm). The initial crack length (a_0) was 0.66 *L*, where *L* corresponds to half of the support span (125 mm). The film-bonded plates were vacuum bagged and finally cured at 120 °C. The fabricated joined plates were water jet cut to 15 mm wide specimens with dimensions as depicted in Fig. 1.

2.2. Mechanical testing

The experimental test setup is presented in Fig. 2. A servo-hydraulic universal testing machine (Instron, 8800) with a 100 kN load sensor was used to induce the cyclic loading. First, a quasi-static ENF test at a test rate of 5 mm/min was carried out. Then, force-controlled fatigue tests at three different loading levels were performed. The maximum load in the static ENF test was 9674 N, and the fatigue tests were then carried out using a load level of 50%, 60% and 70% of the static maximum force (Fig. 3). The slight nonlinearity in the load-displacement curve prior to the load maxima is presumably due to the initiation of the plasticised region's formation at the pre-crack tip. Three specimens were tested per loading case. The applied *R*-ratio was 0.1, which was used to avoid total load removal because it is known to decrease the specimen's movement in the test jig. The loading spectrum (waveform) consisted of a repeating series of 16 sinusoidal cycles at the frequency of 4 Hz followed by a 1-s static hold at the maximum force (Fig. 3), which was first screened to be suitable parameter spectrum in terms of the performance of the used measurement devices. It should be noted that the spectrum must have the short hold at the maximum load at selected cycle intervals, otherwise the type of cycling can be chosen freely.

2.3. Fracture surface characterisation

The fatigue tests were run until the crack in the adhesive layer had visually propagated near the central loading pin. After the fatigue tests, the adherends were manually torn apart, and the fracture surfaces were studied visually. For two of the fatigue tests, the loading was stopped after the visually-observed crack had propagated several millimetres. The cracked area of the specimens was studied using a penetrating fluid (MR® 68NF, MR® Chemie GmbH, Germany). The penetrating fluid was applied by spraying it over the same surface of the specimen observed during the fatigue test (for crack propagation). The excess penetrating fluid was wiped off after 10 min, and the developer fluid was sprayed on the surface. The adherends were torn apart, and the developer fluid was sprayed onto the revealed fracture surfaces. Finally, the fracture surfaces were studied using the optical profilometer (Alicona InfiniteFocus G5, Bruker).

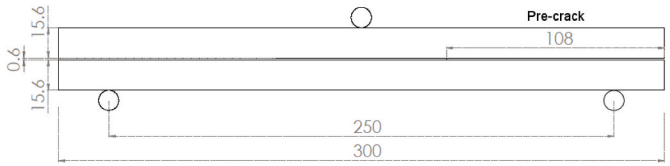

Fig. 1. The ENF specimen's dimensions (in mm) in this study.

Fig. 2. The experimental test setup in this work.

2.4. Equivalent crack length concept

The crack length during the tests was determined using the equivalent crack length-based theorem [19–21]. In the theorem, instead of trying to detect the visible changes in the crack length (*a*), the effective equivalent crack length (a_e) is used to characterise the crack propagation. The equivalent crack length is calculated utilising the changes in the specimen compliance as the crack propagates. The equivalent crack takes, by theory, into account not only the distinct observable visual crack length but also considers the effect of the FPZ ahead of the distinct crack tip. The FPZ, in the vicinity of the crack tip, is difficult to observe visually, but it affects the material's mechanical performance. Thus, FPZ also affects the compliance of the specimen that is being measured. The equivalent crack length was determined using the Compliance-Based Beam Method (CBBM) [22] as

$$a_e = a + \Delta a_{FPZ} = \left[\frac{C_{corr}}{C_{0corr}} a_0^3 + \frac{2}{3}\left(\frac{C_{corr}}{C_{0corr}} - 1\right) L^3\right]^{1/3} \quad (1)$$

where

$$C_{corr} = C - \frac{3L}{10Gbh} \text{ and } C_{0corr} = C_0 - \frac{3L}{10Gbh} \quad (2)$$

In the above equations, *C* and C_0 denote the current and initial (i.e. pre-crack state) compliances of the specimen determined from the load and mid-point deflection data. a_0 is the initial crack length, *L* is the span length of the specimen, and *G*, *b* and *h* are the shear modulus, the width, and the height of the single adherend, respectively. When using the CBBM, a_e is evaluated purely from the load-deflection data, excluding the need to measure any exact crack length.

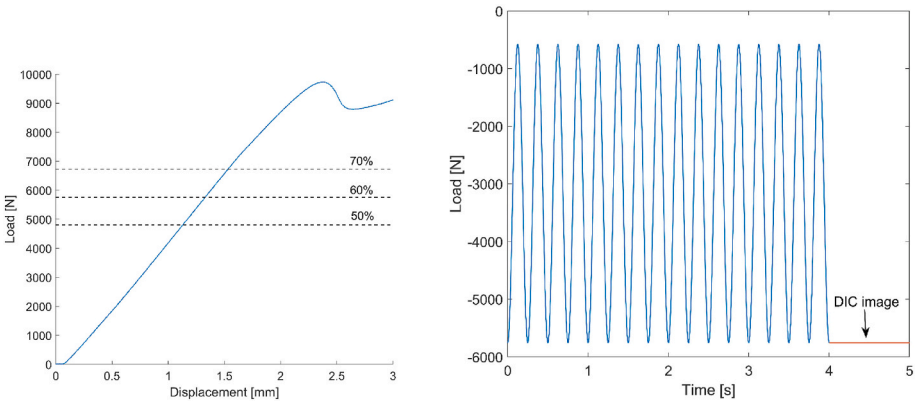

Fig. 3. a) The maximum compression loads used in the sinusoidal loading applied in fatigue testing based on the load-displacement curve of the quasi-static ENF test. b) The repeating unit of the loading spectrum for the 60% loading case.

2.5. Digital image correlation

A three-dimensional DIC setup was used to study the adherends' deformation in a specified (surface) area between the central loading pin and the initial pre-crack. The DIC method is based on tracking the movement of small facets (subsets) to which the studied digitised surface images are divided [23]. The locations of the identified subsets are tracked from image to image using so-called correlation algorithms. From the result, the full-field displacement vectors of the studied surface can be calculated. The resulting full-field data can finally be derived into the desired quantity of interests, such as strains or velocity.

Each subset must have a unique pattern to be distinguishable from the other identified subsets. In order to accomplish this, a thin random black and white pattern was applied over the selected ENF specimen's surface using matt paints and foam rollers. The 3D DIC system consisted of two 5 MP cameras with 50 mm objectives (using an aperture of F11) and pulsed LED flashes. The recording rate was 0.2 Hz, and the image exposure time was synchronised with the test machinery so that an image pair with the two cameras were taken at every static hold step at the maximum load and throughout the fatigue test (see Fig. 3). The calibrated setup resulted in a scale factor of 0.0236 mm/px. The DIC analysis with the images was carried out using Davis 10.0.5 software (Lavision, Germany). The matching criterion was the zero-normalised sum of squared difference (ZNSSD), and affine shape functions were allowed for the subsets. A 6th-order spline was used as the interpolation method. The subset and step sizes were screened first to achieve good spatial resolution and, simultaneously, to keep the noise at a reasonable level. Finally, 35 px and 11 px values were used in the analysis.

2.6. Post-processing of DIC data for crack length

The specified area of interest was selected to cover the area between the central loading pin and the pre-crack tip, i.e. the region where the crack can propagate during a test. The 3D DIC provides the full displacement and strain fields over this area. However, due to the large field-of-view and the resulting mm-to-pixel scale factor, the DIC setup and the analysis parameters yielded a larger virtual strain gauge size (VSG) (57 px or 1.34 mm) than the thickness of the adhesive layer. In other words, the spatial resolution of the applied setup was too low to measure the actual strain values directly (in a reliable manner) in the adhesive. A small VSG size, close to the used thickness of the adhesive layer, could have been achieved by decreasing the subset and step sizes during the analysis. However, it is challenging to ensure that the strong deformation gradients at the adhesive-adherend interfaces, and the damaged adhesive region in front of the distinct crack would not have specimen-wise effects on the derived DIC-based strain values in the specimen. Also, decreasing the subset size will result increased noise in the derived strain. Because an automated and objective method for monitoring the crack propagation was aimed, as presented schematically in Fig. 4, the direct method to derive the crack tip position basing on the DIC-based strain field was not considered feasible.

Fig. 5a depicts the patterned surface of an ENF specimen, which shows the pre-crack location and the approximate location of the instantaneous crack tip in a fatigue test. Visually defining the exact crack tip location is difficult, if not impossible. This is especially true in mode II dominant tests, although the applied thin white paint over the specimen surface makes the visual detection slightly easier (than without any paint). Instead of studying the computed strains directly in the adhesive layer, the developed crack tip detection method is based on measuring the local displacement vectors of both adherends (upper and lower) near the adhesive layer. More precisely, the displacement vectors of the two adherends are derived along two lines (of data collection) defined by an equal distance from the adhesive layer's centre line (here 1 mm), as presented in Fig. 5a. A recent study used a similar technique to determine the shear and opening strains of the adhesive layer under a mixed-mode loading [18].

The method of defining the crack tip location is illustrated in Fig. 5b. Fig. 5b shows the displacement in the y-direction (vertical) for the upper and lower adherends after the first block of the repeating cycles of the test (i.e. initial), and after 3000 cycles. A video presenting the adherends' displacement over a single fatigue test is found in the Supplementary data. The separation ($\Delta d = d_{upper} - d_{lower}$) between the displacements of the upper and lower adherends is determined along the whole adhesive line (inside the specified area of DIC measurement). In the beginning of a test, the initial pre-crack tip location can be visually observed (confirmed). The separation in the adherends' deformation at the pre-crack location, under the initial hold at the maximum force after the first block of cycles, is used as the definite threshold value representing the crack position. This threshold is used to determine the DIC-based crack length or, in other words, the position of the DIC-based equivalent crack tip location.

A MATLAB script was written to find, from each curve, the 'horizontal' location (x), where the same Δd is observed as at the pre-crack tip at the start of the test (hold at the load maxima). Both the separation of sliding (x-direction) and opening (y-direction) deformations, as the basis for the crack tip detection, were studied. It should be noted that the curvature of the specimen was not taken into account here. Still, its effect on the determined displacements at the adherends' surfaces (in the specified region) can be considered negligible due to the large radius of the specimen curvature.

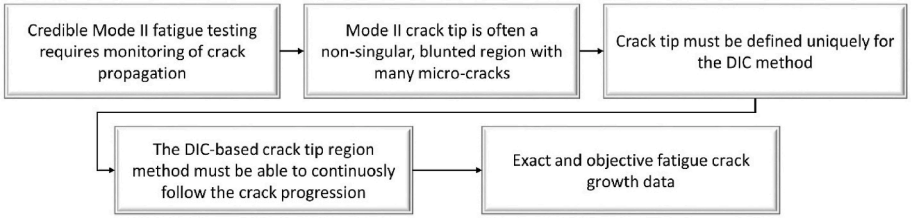

Fig. 4. The targets and requirements in steps to determine crack growth with a DIC concept.

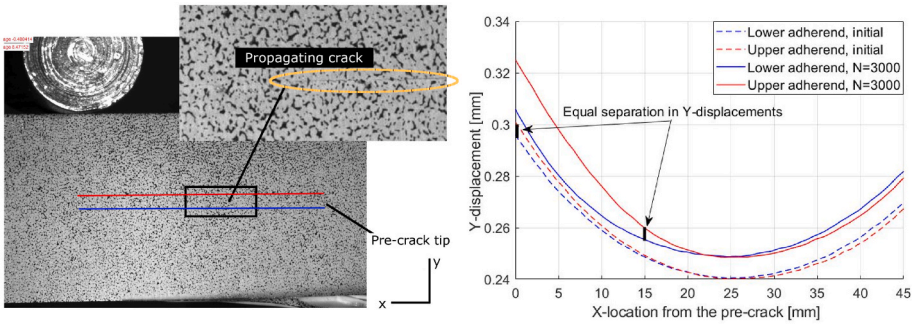

Fig. 5. a) A propagating crack during a fatigue test (the specimen with a DIC pattern). The red and blue lines show the data collection along which the adherend's displacement for further DIC analysis is exported. b) The principle for the method is to determine the instantaneous crack location from the adherend's (opening) displacement. The 'initial' refers to the measured status at the first hold in the load maxima (i.e. cycles = N = 16).

3. Results and discussion

3.1. Fracture surfaces and penetrating fluid experiments

The fatigue tests were continued until the crack, by visual observation, propagated right below the central loading pin. All the specimens, the glued adherends, were torn apart after testing, and the fracture surfaces were optically studied. Representative fracture surfaces for three different fatigue load levels are shown in Fig. 6. In addition to the tested specimens, a fracture surface after a quasi-static ENF test is shown for comparison.

The pre-crack was formed between two layers of film adhesive during the specimen fabrication. The fracture surfaces indicate that the crack propagated closer to the upper adherend (surface), as observed similarly in other studies [24]. In most of the specimens, the crack found its way from the adhesive layer's centre line towards the upper

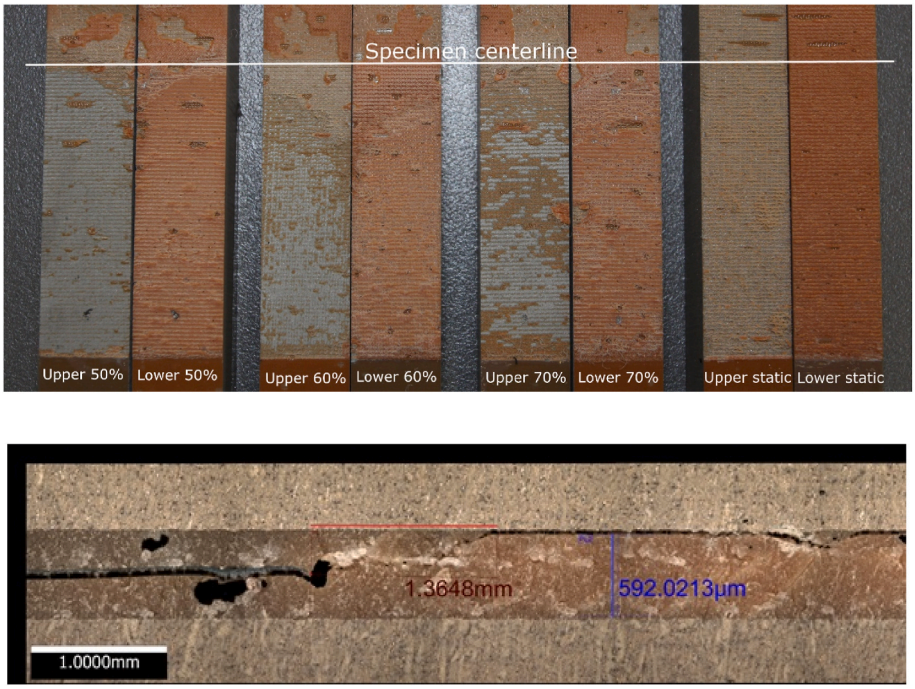

Fig. 6. (Above) The fracture surfaces of the fatigue-tested specimens (load levels of 50%, 60%, 70%) and a quasi-static tested ENF specimen. (Below) An optical image is taken from a cross-section of a tested specimen (50%). The red bar presents the approximate distance (1.365 mm) from the pre-crack tip to the stable crack path point near the upper adherend. The blue line presents the thickness of the adhesive layer (0.592 mm).

adherend's surface just after a few millimetres of propagation (Fig. 6). Although the fracture propagated very near the upper adherend, the failure mode is still cohesive for every test based on adhesive residue.

Two fatigue tests at the load level of 60% were stopped before the visually detected crack propagation below the central loading pin. The first test was stopped after 1500 cycles, and the second after 2000 cycles. These specimens were studied using the penetrating fluid method, and the analysis images are shown in Fig. 7. The pre-crack tip is located on the right-hand side of the image, and the crack has propagated to the left. The fracture surfaces of the specimens can be divided into three regions: 1) the white region on the left, 2) the pink-tinted region in the middle, and 3) the dark purple region on the right. The white colour indicates the fracture surface where the penetrating fluid had not migrated, i.e. where the adhesive had been entirely intact when the penetrating liquid was applied. The dark purple colour indicates the region where the penetrating liquid had flown readily, i.e. there was a distinct crack. In the pink-tinted region, the assumption is that the amount of the penetrating liquid had been significantly lower than the location of the distinct crack with the well-penetrating liquid. However, as some liquid had penetrated through the specimen in the width direction (from one surface and up to the opposite surface), there must have been continuous cracks (or micro tunnels) throughout the adhesive layer in the width direction of the specimen. The lengths determined based on the colour categories are presented in Table 1. The observed non-uniformity of the pink-tinted region, in the width direction of the specimens, is presumed to have formed due to fabrication-based voids in the adhesive layer.

3.2. Results based on the compliance-based approach

When the crack propagates, it results in a decrease in the bending stiffness of the ENF specimen. Thus, crack propagation increases the specimen's measured compliance. As the tests here were performed with the force-controlled movement, the deflection of a specimen increases with the crack propagating. An example of the change in the mid-point-related deflection (measured at the point of maximum force per cycle) is shown in Fig. 8a. The equivalent crack length curves for different load levels, determined by using the compliance measurements and Eq. (1), are depicted in Fig. 8b. The tests were stopped intentionally when the crack was visually estimated to be propagated near the central loading pin.

In general, the shape of the curves remains similar, and the decrease in load level shifts the equivalent crack length towards a higher cycle count. The specimen-wise scatter in the crack propagation behaviour increases with the decreased load level. The curves show that, for approximately the first 5 mm, the value of a_e propagates with a highly nonlinear growth rate. After this regime, the crack propagates at a steadier rate until a_e reaches approximately 22–25 mm. Basically, this crack (length) shows the point where the compression—caused by the central loading pin—starts to cause compressive normal stress at the adhesive. This behaviour has been explained to hinder self-similar crack growth [10]. The compression in the loading direction can also be seen in Fig. 5b, where the deformation curves of the adherends, determined using the DIC-based displacements, are shown. The normal stress at the adhesive changes from small tensile stress to compressive stress at a distance of approximately 22 mm from the pre-crack. In addition, this location is near the point of the ultimate valley of the deformed shape of the specimen under bending.

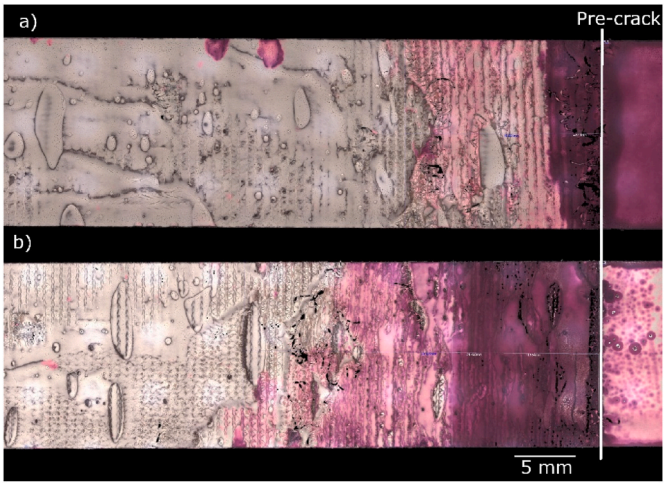

Fig. 7. The fracture surface of a fatigue test specimen after the adherends have been torn apart (60% load level) and after the application of penetrating fluid. Two examples are shown: a test stopped after a) 1500 cycles, and a test stopped after b) 2000 cycles.

Table 1
The crack lengths determined with different methods for the specimens stopped after 1500 and 2000 loading cycles.

Specimen	Penetrating fluid, purple (crack) area [mm]	Penetrating fluid, pink-tinted (microcracked) area [mm]	Effective crack length a_e [mm]	DIC, opening-based [mm]	DIC, shear-based [mm]
Loading 60%, 1500 cycles	4–5	17	3.5	19	7
Loading 60%, 2000 cycles	11–13	22–32	10	30	21

3.3. Results based on the DIC-based approach

Fig. 9 shows the progression of the determined separations (Δd) determined from the opening and shear deformation data (i.e. in y- and x-directions of the adherends) along the adhesive line during a fatigue test. The black dots in Fig. 9 present the points for a proceeding test, where Δd (either opening or shear direction) having the defined threshold value representing the crack tip is observed. To sum up, this data presents the location maps where the deformation state at the adherends (over a test) is similar to the initial condition (at the vicinity of the pre-crack location).

At the beginning of a test, the opening-related Δd is naturally very small. Still, as the test proceeds, a more prominent separation is formed, and the curves' shape changes. Fig. 9b shows the procedure results but determined from the shear deformation (namely based on the displacements in the x-direction).

3.4. Sensitivity of the DIC-based approach

Fig. 10 depicts the determined crack propagation using the opening and shear data versus the cycle count for a median specimen (60% load level). It is interesting to see the effect of the threshold on the detected crack length, which was used to define the original crack tip. The separation value (Δd) for the pre-crack location, after the first repeating loading cycle ('Initial' point), is the reference against which the accumulating data is analysed in the method. The crack-defining threshold can technically be freely selected. The results show that the method, when based on the shear separation, is highly sensitive to the used threshold value. However, the effect is much less for the crack length by the opening-based data.

The normal strain (in the y-direction, matching the loading direction) in the aluminium adherend is negligible during the bending of the ENF specimen in this study. Therefore, the measured displacement separations (Δd values) in the y-direction due to the progressing crack in

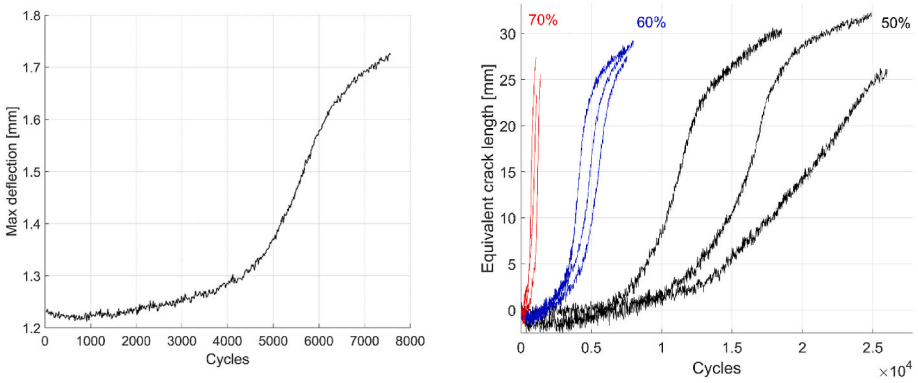

Fig. 8. a) An example for the maximum deflection data of the specimen's (60% load level) middle point versus the cycle count. b) The equivalent crack length (a_e) for different load levels.

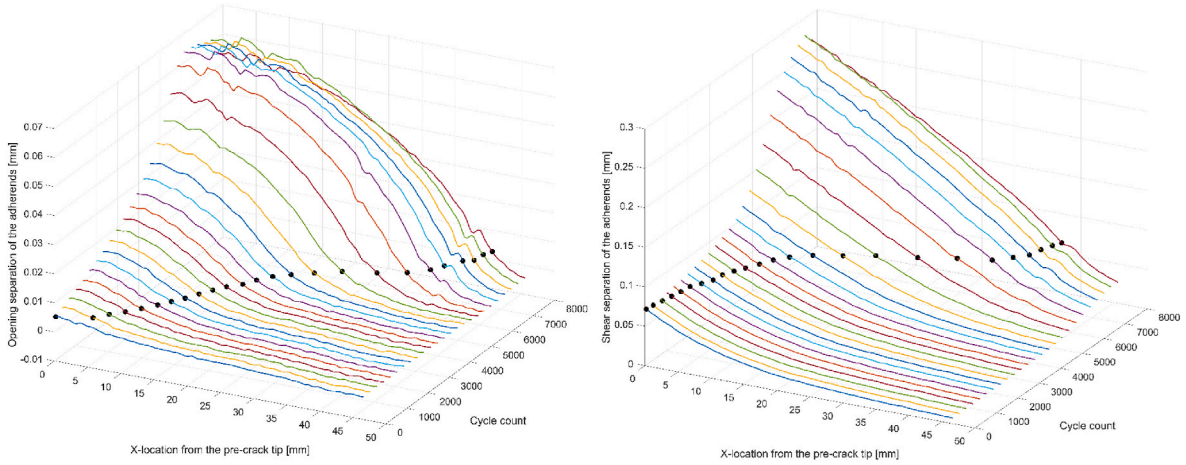

Fig. 9. Displacement separation curves along the adhesive (line) as a function of cycle count (60% load level). The black dots present the location of the instantaneous equivalent crack tip defined based on the initial separation threshold based on a) opening and b) shear displacement.

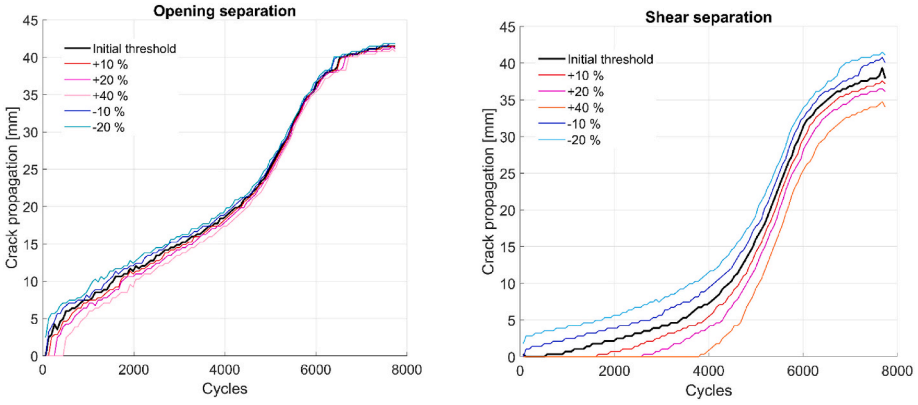

Fig. 10. Crack propagation curves and the effect of the crack-defining threshold when using a) the opening data; b) the shear data (60% load level).

the adhesive originate practically only due to the changes in the adhesive layer. Thus, the exact (y-) distance of the extracted displacement vectors at the adherends (distance from the adhesive centre line) has an insignificant effect on the DIC-based method when using the opening data. This is illustrated in Fig. 11, where the crack propagation length, obtained using the adherend deformations extracted at two different (y-) distances (1 mm and 3 mm), are shown. Again, the shear data-based results show a high sensitivity for the selected distance.

The minimum distance where the adherend displacements can be derived is significantly affected by the parameters used in the DIC analysis and, especially, by the subset size. Basically, the distance must be more than half of the adhesive thickness plus half of the subset size (here 0.71 mm). When this condition is fulfilled, the local displacement information for the DIC analysis is obtained only on (pixels of) the aluminium adherend outside the adhesive-adherend interface (affine deformations assumed).

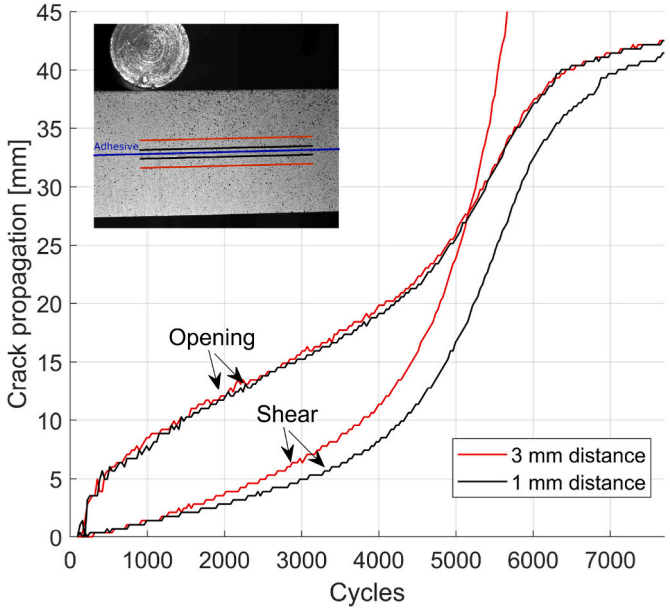

Fig. 11. The effect of the selected extraction distance, measured from the adhesive layer's centre line, on the crack propagation. The effect is shown for data related to opening and shear deformation.

3.5. Comparison of the approaches to detect the crack length

The crack lengths determined using the two approaches for a typical (median) test specimen (at 60% load level) are shown in Fig. 12. The trend of all the curves is similar, resembling an S-curve. In these S-curves, a clear increase in the crack propagation rate is detected after the first essentially linear propagation phase. However, the crack propagation curves between the DIC and CBBM approaches still differ significantly.

Although challenging, by careful pure visual observation of the recorded (camera) images, the position of the crack tip or, at least, the plasticised adhesive can be manually estimated at the painted specimen surface. This basically forms a third method of determining the crack length. By comparing the methods, the visual observation of the crack matches best with the DIC-based method using the opening

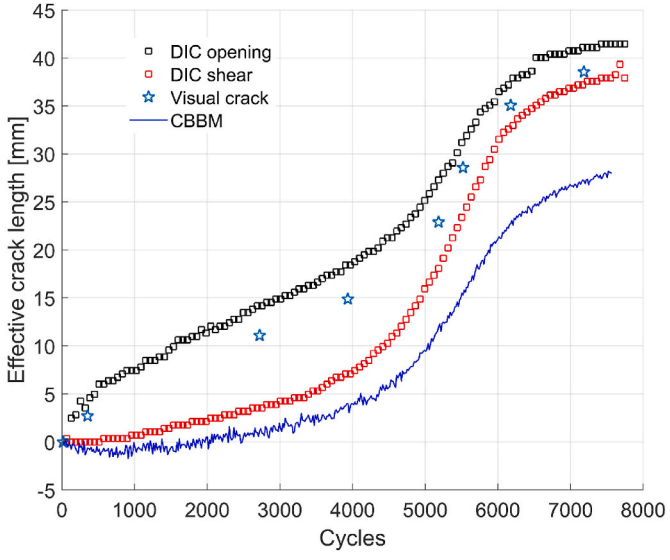

Fig. 12. Comparison of the crack propagation (length) determined with three different methods.

displacement data. On the other hand, the shear displacement-based DIC method matches quite accurately with the CBBM results. The CBBM shows the shortest determined crack length.

The crack lengths of the tests stopped after 1500 and 2000 cycles, determined with the different methods, are shown in Table 1. It can be seen that the CBBM results in comparable values with the values obtained via the analysis of penetrating fluid. More specifically, the data matches the dark purple region in Fig. 7. The opening data-based DIC resulted in comparable values with the pink-tinted region. The crack lengths detected with the different techniques for the specimen loaded for 2000 cycles are illustrated in Fig. 13, together with optical microscopy images. The distinct crack, close to the upper adherend (seen in close-up 2), is visible approximately to the same point (distance) as given by the compliance-based equivalent crack length (point B). The region between this point (point B) and the point given by the length result of the opening data-based DIC method (point E) shows a clear repeating, inclined cracking pattern in adhesive. Basically, this region also corresponds to the pink-tinted region observed using the penetrating fluid.

According to the results, the developed opening-based DIC method reveals thus the region of the adhesive, in which permanent damages in the adhesive have occurred due to the cycled loading. On the other hand, the length of the distinct, continuously open crack can be estimated well with the CBBM. The shear-based DIC method seem to correlate with the CBBM, but the method is highly sensitive on the analysis parameters hindering its use. The considered methods to monitor the progressing crack in fatigue loaded ENF test are summed up in Fig. 14.

3.6. Remarks on the DIC-based opening separation

The opening (between adherends) in an ENF test is not intuitive when pure mode II loading is considered. However, small 'opening' deformations have been documented originating from the phenomena due to the micro-cracked and segmented adhesive [25], and the roughness of the fracture surfaces [21]. Basically, non-zero damage (preceding the crack tip) and Poisson's ratio less than 0.5 of the adhesive will also have to open the stiff adherends after cracking. The opening deformations observed by DIC can also partly be explained by contact surface roughness when there is no perfect match in the contact of the adherend surfaces encountering shear-induced sliding. The ENF specimen has a pre-existing crack tip made by a release film strip. Based on our observations, it is pretty typical that the fabricated pre-crack plane has some waviness. The waviness is formed due to the unbalanced shrinking of the (PTFE) release film during the adhesive curing process. This waviness at the specimen end region can clearly be detected after tearing apart the adherends, as depicted in Fig. 15. It should be noted here that the opening by the waviness balances out when the

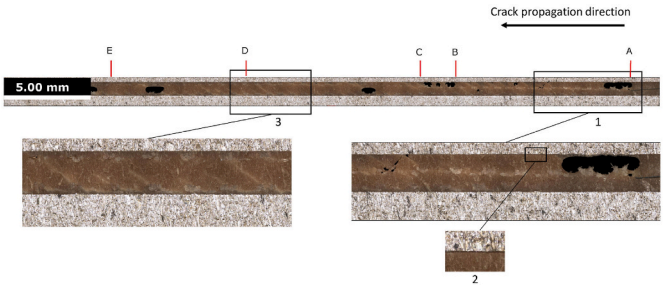

Fig. 13. An optical image of the adhesive layer after the fatigue-tested specimen showing various locations for the detected crack (lengths) with different methods. The loading level was 60%, and the test was stopped after 2000 cycles. A = pre-crack location, B = effective crack length, C = crack with penetrating fluid and purple colour, D = the minimum length of 'FPZ' with penetrating fluid creating a pink-tinted region and E = crack length with DIC opening-based data.

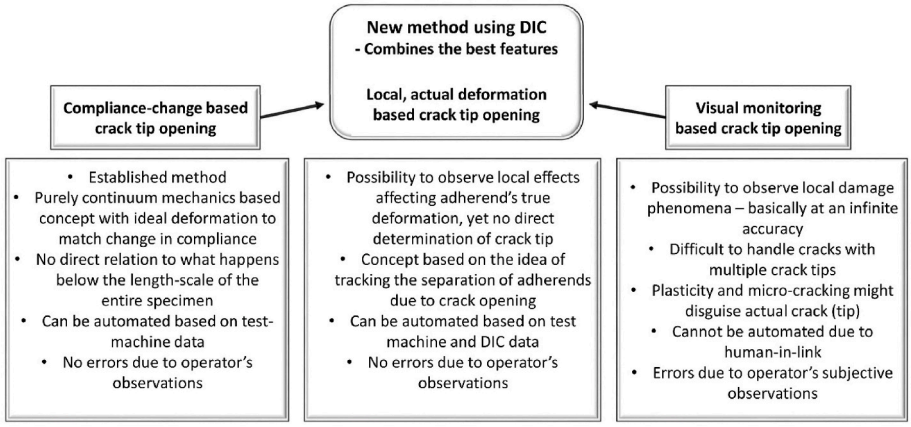

Fig. 14. Summary of the compared methods for the crack tip monitoring in ENF fatigue test.

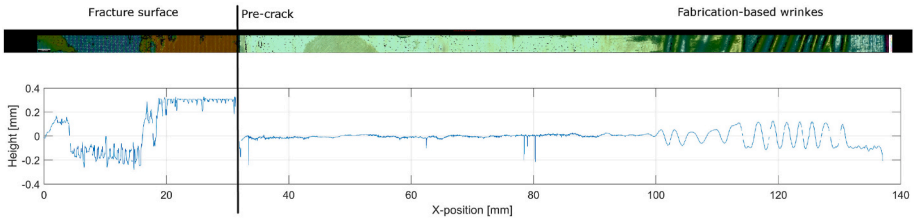

Fig. 15. A profilometer image of a lower adherend's portion of the fracture surface (top) and the line contour shows the height profile (bottom). The right-hand edge is the specimen end, and the crack has propagated to the left from the pre-crack.

crack-defining threshold is selected specimen-wise in each test.

3.7. Formation of the fracture process zone (FPZ)

The FPZ is the established designation to define the non-negligible region ahead of the distinct crack tip where the material has already undergone softening damage. The damage can happen by different means, including plastic deformation, microcracking, crack-branching, microvoid formation and possible fibre bridging [22,26,27].

The results of this study revealed that extensive microcracking was prominent in the adhesive layer after testing (the inclined cracks in Fig. 13). The woven carrier is a feature of the adhesive film product that can increase the likeliness of microcracking. It is suggested here that the interfaces between the filaments of the polyester carrier and epoxy are prone to microvoids. In practice, microcracking and damage function as the desired toughening mechanism and also increases the size of the FPZ.

The microcracked region was visually detected here during and after the tests. However, accurate length measurement for FPZ is ambitious. The penetrating fluid indicated a rather distinct region between the open crack (purple colour) and the undamaged region. It is suggested here that this region (the pink-tinted region) is the microcracked region.

Due to the FPZ, unambiguous detection of any 'true' crack length is practically impossible [3]. Eventually, this fact complicates the analysis of the ENF tests since the size of the FPZ affects the resolved fracture energy. The effective crack length (a_e) determined with the CBBM includes, by theory, also the FPZ because the derivation of a_e bases on the measured (real) changes in the flexural rigidity of the ENF specimen (including the FPZ) [22,28].

3.8. Separated adherend zone (SAZ)

The DIC-based method presented here analyses crack propagation according to the measured adherends' separation. The determined (crack) length for opening data, i.e. the separated adherend zone (SAZ), shall be distinguished from the CBBM results with the FPZ. From the mechanical point of view, the SAZ, depending on the threshold and for the ENF specimen, makes the separation of the adherends more prominent whenever damage or plastic deformation of adhesive occurs. With the current formulation, the SAZ does not distinguish if the separation is due to the propagation of any 'true' crack or the expanded plasticised or damaged region in the adhesive layer. The penetrating fluid, however, indicated a good correlation between the length with the microcracked region and the SAZ.

Fig. 16a depicts the effective crack length curves (60% load level) determined by the CBBM and DIC-based methods. The difference between the two methods is presented in Fig. 16b. The result suggests that the SAZ begins to develop first. It is presumed to originate due to the plastic deformation and microcracking of adhesive ahead of the originally blunt pre-crack tip (i.e. nucleation). However, this first phase does not affect the measured compliance (within experimental scatter) nor the effective crack length a_e by the CBBM. When the SAZ reaches 11 mm, the effective crack length determined by the CBBM increases, this increase is assumed to originate due to the formation of a coalesced crack in the adhesive (near the upper adherend surface in this study). Thereafter, the FPZ and the SAZ increase at different rates. The difference curve (Fig. 16b) indicates that the length of the SAZ (in front of the FPZ) increases as the test proceeds. This indicates that the length of the deformed adhesive (its zone ahead of the crack) is not exactly stable, but increases as the crack propagates during an ENF test.

In Fig. 16b, a clear change in the curve is observed at 4000 cycles, which equals the SAZ and FPZ lengths of 24 mm and 6 mm, respectively. The distance of 24 mm is also the location of the valley point in the deformed shape of the ENF specimen because of the unsymmetrical deformation due to the pre-crack (Fig. 5). Around this valley point, the value of normal strain in the loading direction in the adhesive layer changes from tensile strain to compressive strain. The observation indicates that when the microcracked adhesive region propagates and reaches the valley point of the bent specimen, the slope of the crack propagation rate determined by either of the methods significantly

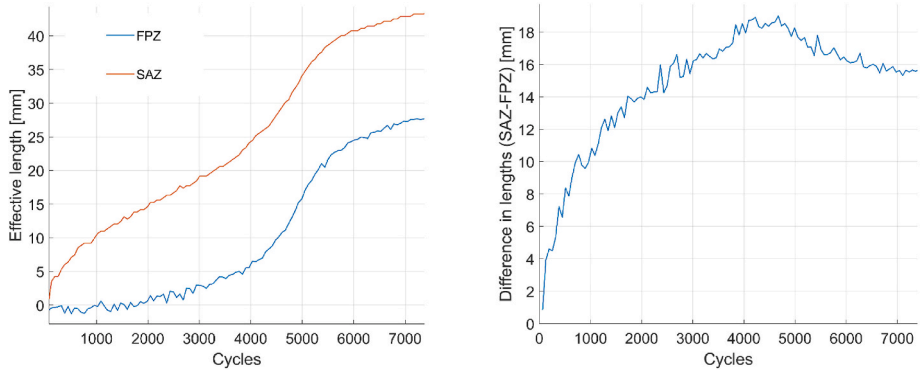

Fig. 16. a) Determined effective crack lengths with the FPZ (by the CBBM) and SAZ (by the DIC-based adherend opening). b) The difference between the CBBM and the SAZ-crack lengths.

increases. The behaviour was similar in all the tests with different load levels. Therefore, the development of the damaged or plasticised adhesive region tends to affect the crack propagation rate of the 'distinct' crack determined by the CBBM.

4. Conclusion

The work focused on characterising crack propagation in FM 300-2 epoxy adhesive film under fatigue loading using the ENF specimen. The crack propagation in the ENF test is shown as sliding at the debonded interface when there is mode II loading. The sliding is exceptionally challenging to observe visually. Moreover, the precise crack length definition is not unambitious due to the damaged large region ahead of the distinct crack. In this work, the applicability of a DIC-based approach is developed and analysed in detail. Instead of aiming to detect the distinctly visible crack, the new approach uses the adherends' deformation to define the damaged region in the adhesive by studying the introduced specimen's separated adhesive zone (SAZ). The applicability of both opening (vertical) and shear (horizontal) deformation of the adherends was considered. The reference results were provided with the established CBBM method. In addition to the developed approach and the CBBM, penetrating fluid measurements were performed to study the developed crack in the adhesive layer.

Based on this work, the following conclusions can be made:

- The DIC measurements indicated small opening deformation between the adherends of the ENF specimen. The observation was used in defining the damaged adhesive region in the specimen.
- The crack monitoring was achieved with the established SAZ-defined crack tip.
- The DIC-based method estimates a larger crack length than the CBBM.
- The penetrating fluid measurements indicated two different regions at the specimen fracture surface. The intensively penetrated region agreed with the CBBM results and was verified as the distinct crack length. The less penetrated region agreed well with the DIC method with the opening data and is suggested to denote the damaged microcracked adhesive in ahead of an open crack tip.
- The length of the microcracked region ahead of the distinct crack increases as a fatigue test proceeds. However, it does not obviously affect the compliance of the bent ENF specimen. On the other hand, its size was eventually observed to affect the propagation rate of the distinct crack in fatigue-loaded ENF specimens.

Declaration of competing interest

The authors declare that they have no known competing financial interests or personal relationships that could have appeared to influence the work reported in this paper.

Data availability

Data will be made available on request.

Acknowledgements

This work was funded by the financial support of the Finnish Defence Forces Logistics Command.

Appendix A. Supplementary data

Supplementary data to this article can be found online at https://doi.org/10.1016/j.ijadhadh.2023.103332.

References

[1] ISO 25217:2009. Determination of the mode 1 adhesive fracture energy of structural adhesive joints using double cantilever beam and tapered double cantilever beam specimens. Int. Organ. Stand. 2009;1:1–24.
[2] Floros IS, Tserpes KI, Löbel T. Mode-I, mode-II and mixed-mode I+II fracture behavior of composite bonded joints: experimental characterization and numerical simulation. Compos B Eng 2015;78:459–68. https://doi.org/10.1016/j.compositesb.2015.04.006.
[3] Blackman BRK, Kinloch AJ, Paraschi M. The determination of the mode II adhesive fracture resistance, GIIC, of structural adhesive joints: an effective crack length approach. Eng Fract Mech 2005;72:877–97. https://doi.org/10.1016/j.engfracmech.2004.08.007.
[4] Bernasconi A, Beretta S, Moroni F, Pirondi A. A study on fatigue crack propagation in thick composite adhesively bonded joints. In: 18th Eur. Conf. Fract. Fract. Mater. Struct. From micro to macro scale; 2010. p. 1–8.
[5] Madhusudhana KS, Narasimhan R. Experimental and numerical investigations of mixed mode crack growth resistance of a ductile adhesive joint. Eng Fract Mech 2002;69:865–83. https://doi.org/10.1016/S0013-7944(01)00110-2.
[6] Krenk S, Jonsson J, Hansen LP. Fatigue analysis and testing of adhesive joints. Eng Fract Mech 1996;53:859–72.
[7] Wong L, Chowdhury N, Wang J, Chiu WK, Kodikara J. Fatigue damage monitoring of a composite step lap joint using distributed optical fibre sensors. Materials 2016;9. https://doi.org/10.3390/ma9050374.
[8] Chaves FJP, da Silva LFM, de Moura MFSF, Dillard DA, Esteves VHC. Fracture mechanics tests in adhesively bonded joints: a literature review. J Adhes 2014;90:955–92. https://doi.org/10.1080/00218464.2013.859075.
[9] Blackman BRK, Brunner AJ, Williams JG. Mode II fracture testing of composites: a new look at an old problem. Eng Fract Mech 2006;73:2443–55. https://doi.org/10.1016/j.engfracmech.2006.05.022.
[10] Fernández MV, De Moura MFSF, Da Silva LFM, Marques AT. Characterization of composite bonded joints under pure mode II fatigue loading. Compos Struct 2013;95:222–6. https://doi.org/10.1016/j.compstruct.2012.07.031.
[11] de Moura MFSF, Gonçalves JPM, Fernandez MV. Fatigue/fracture characterization of composite bonded joints under mode I, mode II and mixed-mode I+II. Compos Struct 2016;139:62–7. https://doi.org/10.1016/j.compstruct.2015.11.073.
[12] Olajide SO. Progress on investigation on damage analysis in bonded polymer composites under fatigue. Int J Fatig 2017;96:224–36. https://doi.org/10.1016/j.ijfatigue.2016.12.016.
[13] Pérez-Galmés M, Renart J, Sarrado C, Brunner AJ, Rodríguez-Bellido A. Towards a consensus on mode II adhesive fracture testing: experimental study. Theor Appl Fract Mech 2018;98:210–9. https://doi.org/10.1016/j.tafmec.2018.09.014.

[14] Orell O, Vuorinen J, Jokinen J, Kettunen H, Hytönen P, Turunen J, Kanerva M. Characterization of elastic constants of anisotropic composites in compression using digital image correlation. Compos Struct 2018;185. https://doi.org/10.1016/j.compstruct.2017.11.008.
[15] Janeliukstis R, Chen X. Review of digital image correlation application to large-scale composite structure testing. Compos Struct 2021;271:114143. https://doi.org/10.1016/j.compstruct.2021.114143.
[16] Ghaednia H, Cermik O, Marghitu DB, Kardel K. Collision measurements using digital image correlation techniques. Int J Mech Sci 2017;131–132:836–46. https://doi.org/10.1016/j.ijmecsci.2017.07.025.
[17] Sun G, Liu X, Zheng G, Gong Z, Li Q. On fracture characteristics of adhesive joints with dissimilar materials – an experimental study using digital image correlation (DIC) technique. Compos Struct 2018;201:1056–75. https://doi.org/10.1016/j.compstruct.2018.06.018.
[18] Jokinen J, Orell O, Wallin M, Kanerva M. A concept for defining the mixed-mode behaviour of tough epoxy film adhesives by single specimen design. J Adhes Sci Technol 2020:1–18. https://doi.org/10.1080/01694243.2020.1746606.
[19] De Moura MFSF, Gonçalves JPM, Chousal JAG, Campilho RDSG. Cohesive and continuum mixed-mode damage models applied to the simulation of the mechanical behaviour of bonded joints. Int J Adhesion Adhes 2008;28:419–26. https://doi.org/10.1016/j.ijadhadh.2008.04.004.
[20] de Moura MFSF, de Morais AB. Equivalent crack based analyses of ENF and ELS tests. Eng Fract Mech 2008;75:2584–96. https://doi.org/10.1016/j.engfracmech.2007.03.005.
[21] Yoshihara H, Ohta M. Measurement of mode II fracture toughness of wood by the end-notched flexure test. J Wood Sci 2000;46:273–8. https://doi.org/10.1007/BF00766216.
[22] de Moura MFSF, Silva MAL, de Morais AB, Morais JJL. Equivalent crack based mode II fracture characterization of wood. Eng Fract Mech 2006;73:978–93. https://doi.org/10.1016/j.engfracmech.2006.01.004.
[23] Jones MA, Iadicola EMC. A good practices guide for digital image correlation. Int. Digit. Image Correl. Soc. 2018;94. https://doi.org/10.32720/idics/gpg.ed1.
[24] Dessureault M, Spelt JK. Observations of fatigue crack initiation and propagation in an epoxy adhesive. Int J Adhesion Adhes 1997;17:183–95. https://doi.org/10.1016/s0143-7496(96)00044-9.
[25] Leone FA, Girolamo D, Dávila CG. Progressive damage analysis of bonded composite joints. 2012. NASA/TM-2012-217790).
[26] Majano-Majano A, Lara-Bocanegra AJ, Xavier J, Morais J. Experimental evaluation of mode II fracture properties of Eucalyptus globulus L. Materials 2020;13:1–13. https://doi.org/10.3390/ma13030745.
[27] Arrese A, Insausti N, Mujika F, Perez-Galmés M, Renart J. A novel experimental procedure to determine the cohesive law in ENF tests. Compos Sci Technol 2019;170:42–50. https://doi.org/10.1016/j.compscitech.2018.11.031.
[28] de Moura MFSF, Campilho RDSG, Gonçalves JPM. Pure mode II fracture characterization of composite bonded joints. Int J Solid Struct 2009;46:1589–95. https://doi.org/10.1016/j.ijsolstr.2008.12.001.